Desalination and Water Treatment
www.deswater.com

doi: 10.5004/dwt.2022.28789

271 (2022) 176–191
September

Optimization of diclofenac sodium adsorption onto graphene nanosheets: capacity, kinetics, isotherms and removal

Glauber da Rocha Medeiros[a,*], Adison da Silva Pereira Júnior[b], Felipe Mendonça Fontes Galvão[b], José Heriberto Oliveira do Nascimento[b,c], Juliana Delgado Tinôco[a,d]

[a]*Graduate Program in Sanitary and Environmental Engineering, Technology Center, Federal University of Rio Grande do Norte, Natal, Rio Grande do Norte, Brazil, Tel. +5584998404265; emails: glauber.medeiros.045@ufrn.edu.br (G. da Rocha Medeiros), juliana.tinoco@ufrn.br (D. Tinôco)*
[b]*Research Group in Micro and Nanotechnology Innovation – GPIMN, Department of Textile Engineering, Technology Center, Federal University of Rio Grande do Norte, Natal, Rio Grande do Norte, Brazil, emails: adsonjunior.sk8@hotmail.com (A. da Silva Pereira Júnior), felipe.galvao@goldentecnologia.com (F.M. Fontes Galvão), joseheriberto@ct.ufrn.br (J.H.O. do Nascimento)*
[c]*Graduate Program in Chemical Engineering, Technology Center, Federal University of Rio Grande do Norte, Natal, Rio Grande do Norte, Brazil*
[d]*Laboratory of Water Resources and Environmental Sanitation – LARHISA, Department of Civil Engineering, Federal University of Rio Grande do Norte – UFRN, 3000, CEP 59078-970, Natal, RN, Brazil*

Received 15 December 2021; Accepted 24 July 2022

ABSTRACT

Recently, emerging contaminants have been studied with greater attention due to their growing presence in aquatic environments, medications being one of the major pollutants owing to their global consumption. Among the main pharmaceuticals detected, the anti-inflammatory diclofenac sodium (DS) is considered the most ecotoxic and features on the European list of priority substances for monitoring as part of Water Framework Directive 39/2013. Among the water treatment processes available, adsorption is a highly effective technical and economic alternative. As such, this study aimed to assess DS removal efficiency using graphene oxide (GO) as an adsorbent. DS was analyzed using a central composite design, with four factors: diclofenac sodium concentration (DS_C of 50 to 450 mg L^{-1}), adsorbent concentration (ADS_C of 0.2 to 5 g L^{-1}), contact time (C_t of 5 to 45 min) and pH (5 to 9). The results confirmed the modeling of adsorption capacity, adsorbate removal, pseudo-first-order and pseudo-second-order kinetics, intraparticle diffusion, and Langmuir and Freundlich isotherms. DS demonstrated an affinity for adsorption onto GO nanosheets. Maximum adsorption capacity for GO was 669.50 mg g^{-1} (DS_C of 450 mg L^{-1}, ADS_C of 0.2 g L^{-1}, C_t of 34.3 min and pH 5) obtained by duplicate identification batches. The data also supported the creation of an equation that indicates the adsorbent dose needed for total DS removal (100%) from a solution.

Keywords: Adsorption; Central composite design; Diclofenac; Graphene oxide

* Corresponding author.

1. Introduction

In the field of health, pharmaceuticals are active substances used to explore or modify the physiological system or pathological state of humans or animals, and widely prescribed in the diagnosis, treatment, relief and prevention of diseases [1]. However, although these substances are used for their beneficial effect on patient health, they have become a global environmental problem. Since the mid-1980s, advances in analytical techniques and equipment and research conducted worldwide have detected trace concentrations of pharmaceutical substances such as synthetic hormones, nonsteroidal anti-inflammatory drugs (NSAIDs), β-blockers, analgesics, lipid metabolism regulators, antidepressants and antiepileptics in surface and groundwater, sewage and the public water supply [2–8].

These substances are currently classified as emerging contaminants (ECs), chemicals of natural (hormones, algal toxins and microorganisms) or synthetic origin (medications, personal care products, pesticides, illicit drugs, chlorination by-products, additives and microplastics), not yet covered by specific legislation (monitoring). Although ECs are a large class of substances, they consist largely of pharmaceutical active compounds (PACs).

Of these, nonsteroidal anti-inflammatory drugs (NSAIDs) are sold without a prescription, which directly increases the chances of their consumption by the population. Diclofenac sodium (DS) is one of the world's most widely consumed drugs and accounts for around one third of the NSAID market in 15 countries, with a market share close to that of the three most popular anti-inflammatories combined, namely ibuprofen (11%), naproxen (9.4%) and mefenamic acid (9.1%) [9,10].

Beek et al. [3] compiled data from 1166 academic articles that identified 631 different pharmaceutical substances in environmental matrices in 71 countries. DS was the most recurring substance, found in 50 countries and often at concentrations above 0.1 μg L^{-1}, considered a potential ecotoxicological risk for non-target organisms based on predicted no-effect concentrations (PNECs) [3].

DS is considered the most ecotoxic NSAID, with literature reports of problems such as reduced reproductivity, oxidative stress, hepatoxicity and mitochondrial (cardiac) alterations in laboratory tests with animals under chronic DS exposure [11,12]. Clinical trials in humans also correlated DS use with the onset of gastrointestinal bleeding, cardiac changes and greater risk of death from heart disease [13]. It was also responsible for declining vulture populations in Africa (>62%) and South Asia (>95%) through poisoning after the birds fed on contaminated cattle carcasses [14–16]. These events prompted the inclusion of DS on the first list of potentially hazardous substances under European Union Directive 39/2013, which stipulates a strategic approach to monitoring the compound and cites one of its objectives as fostering the development of new water treatment technologies for the removal of pharmaceutical substances [17].

Praveenkumarreddy et al. [18] studied NSAID removal at wastewater treatment plants (with activated sludge and upflow anaerobic sludge blanket reactor technologies) in southeast India and recorded average removal efficiencies of approximately 99% for aspirin, 72% for naproxen, 62% for ketoprofen, 52% for ibuprofen and only 40% for DS, from initial concentrations (C_i) of 125–184, 11–217, 2–22, 12–68 and 3–41 μg L^{-1}, respectively. In a pilot study, McKie et al. [19] analyzed the removal of the anti-inflammatories naproxen (C_i = 150–390 ng L^{-1}), acetaminophen (C_i = 60–260 ng L^{-1}), ketoprofen (C_i = 140–630 ng L^{-1}) and diclofenac (C_i = 180–290 ng L^{-1}) from natural water and obtained respective removal efficiencies of 52%, 46%, 38% and 36% via conventional water treatment methods (coagulation, flocculation, settling and sand filtration) with a contact time of 15 min, and 78%, 68%, 29% and 8.7% using 3–5 mg Al^{3+} L^{-1} of aluminum sulfate as coagulant in direct biofiltration with a contact time of 10 min and 0.2 mg Al^{3+} L^{-1}. Rigobello et al. [20] analyzed laboratory-scale diclofenac removal in a conventional water treatment process (coagulation, flocculation, settling and sand filtration) using 3.47 mg Al^{3+} L^{-1}, followed or not by preoxidation with chlorine dioxide, and reported respective efficiencies of 0% and 15% with and without preoxidation, both at an initial concentration of 1 mg L^{-1} of DS, pH 6.5, 70 NTU and 20 uH. These results demonstrate that conventional processes used at water (WTPs) and wastewater treatment plants (WWTPs) are not completely efficient at removing pharmaceutical products, especially diclofenac.

The growing problem of pharmaceuticals and updated environmental legislation have prompted the development of end-of-pipe technologies to remove pharmaceuticals from the public water supply, such as catalytic ozonation, photocatalytic oxidation, ultrafiltration, nanofiltration and adsorption, among others [21–31]. A comparative analysis by Boer et al. [32] indicated that ozonation (0.068–0.56 € m^3), photocatalysis (0.76–1.39 € m^3), UV radiation (0.208–0.248 € m^3) and membrane filtration (0.044–0.8 € m^3) involve higher operating costs than those of adsorption (0.035–0.31 € m^3) for micropollutant removal, depending on the configuration of the treatment system. Additionally, with the exception of adsorption, the technologies mentioned are dependent on electrical energy and their complex technology makes them subject to electricity shortages and/or equipment failure, requiring specialized manpower for maintenance. Ozonation, UV radiation and photocatalysis generate by-products and can transform NSAIDs into more toxic compounds, such as monochlorinated compounds and hydroquinone, with as yet unknown effects [28–31,33]. Adsorption is therefore a promising alternative removal technique for pharmaceuticals due to its low technological complexity and cost, the possibility of recovering the adsorbent material and the fact that it does not generate by-products [34].

Although adsorbents such as wood, polymers, clay and resins can be used to remove pharmaceutical compounds dissolved in water, carbon-based adsorbents are the most effective [21,22,25–27,34–37]. With the development of nanotechnology, synthetic carbon compounds are being used in advanced water treatment processes because their characteristics (porosity, hydrophobicity, surface functional groups) make them suitable for the adsorption of micropollutants dissolved in water. One of these materials is graphene oxide, which has attracted the interest of scientists worldwide because the nanometric size and bidimensional structure of graphene results in a larger specific surface area and electrical properties that favor chemical adsorption,

providing high adsorption kinetics, rapid equilibrium rates in solution, greater adsorption capacity, and effectiveness across broad pH and temperature ranges [34,36,37].

As such, the present study aimed to analyze DS removal from an aqueous solution by graphene oxide (GO) adsorption using a central composite design, and simultaneously assess the main variables that influence adsorption and removal capacity, namely adsorbate and adsorbent concentration, contact time and pH, in addition to analyzing adsorption efficiency via Langmuir and Freundlich isotherms and kinetics via pseudo-first-order, pseudo-second-order and intraparticle diffusion models.

2. Materials and methods

2.1. Graphene oxide synthesis

Graphene oxide (GO) was synthesized from purified graphite (Vonder®, Grupo OVD, Brazil) according to the modified Hummers and Offeman method [38], which consists of chemical oxidation of the graphite and the addition of a strong acid solution. For every 1 g of graphite, 0.5 g of sodium nitrate ($NaNo^3$ P.A., ISOFAR, Brazil) and 23 mL of sulfuric acid (H_2SO_4 P.A., Sigma Aldrich – Merck, Brazil) were added. The mixture was submitted to mechanical agitation for 1 h, at 500 RPM and 20°C, and then slowly added with 3 g of solid potassium permanganate ($KMnO_4$ P.A., Sciavicco, Brazil) to ensure the temperature does not exceed 20°C. Next, the mixture was mechanically agitated for 12 h at the same speed, increasing the temperature to 35°C, and the oxidated graphene paste was then diluted in 500 mL of water. The resulting solution was treated with hydrogen peroxide (H_2O_2 30%, ISOFAR, Brazil) to consume any excess reagents and oxidize the structure, and the synthesized products were then washed with a 5% hydrochloric acid solution (37% HCl, Labsynth, Brazil) to remove metal ions and possible impurities. Next, it was filtered, rinsed with water and dried in an oven at 80°C for 6 h.

2.2. Graphene oxide characterization

The morphological and microstructural properties of GO were obtained by scanning electron microscopy with a field emission gun (SEM-FEG) and high-resolution transmission electron microscopy (HRTEM) on an FEI TECNAI G2 F20 microscope operating at 200 kV. The functional groups present in GO were analyzed by Fourier transform infrared spectroscopy in a Shimadzu IRTracer-100 spectrophotometer in the 400 to 4,000 cm^{-1} wavelength range, operating in transmittance mode with an attenuated total reflectance (ATR) detector. The X-ray diffraction (XRD) spectra were obtained under CuKα radiation (λ = 0.15418 nm) at 40 kV and 30 mA, angle range of $5° \le 2\theta \le 80$, 0.02° step size and speed of $1°/min^{-1}$. The lattice effect of the adsorbent was determined by Raman spectroscopy in a Renishaw inVia Raman microscope (United Kingdom). Raman measurements were obtained at an excitation wavelength of 514 nm. The point of zero charge was determined using a potentiometer and adsorbent-to-solution ratio of 1 mg:1 mL, whereby adsorbent fractions were placed in flasks containing aqueous solution at ambient temperature and under different pH conditions (1–6, 8–12), with a contact time of 24 h. The surface area was assessed using the Brunauer–Emmett–Teller (BET) method.

2.3. Batch adsorption study

2.3.1. Solution preparation, experimental procedures and analysis methodology

Batch adsorption experiments were conducted in line with the following protocol: (a) a stock solution (500 mg L^{-1}) was prepared by diluting 0.5035 g of DS (99.3%, Farmafórmula, Brazil) in 1 L of deionized water; (b) adsorption tests were performed in Erlenmeyer flasks containing 20 mL of the solution under different adsorbate and adsorbent concentrations, pH conditions and contact times (Table 1); (c) solutions with different DS concentrations (50, 150, 250, 350 and 450 mg L^{-1}) were obtained by diluting the stock solution; (d) pH was adjusted by adding hydrochloric acid (37% HCl, Labsynth, Brazil) or sodium hydroxide (NaOH P.A., ISOFAR, Brazil) in a solution with 0.025 N deionized water; (e) tests were carried out under ambient temperature on an orbital shaker at 200 RPM and (f) at the end of each test, the sample was filtered through a 40 μm white ribbon qualitative filter (Qualy, Brazil). Residual DS concentration was determined by UV spectrometry at a wavelength of 274 nm. Readings were performed in triplicate.

2.3.2. Study design and model development

A central composite design was used for this phase of the study. This empirical model is based on an iterative method that assesses the individual effects of each variable in order to optimize the process. The central composite design (CCD) used here consisted of four factors: initial adsorbate concentration (mg L^{-1}), adsorbent concentration (g L^{-1}), contact time (min) and pH; with five levels and one response, namely adsorption capacity q (mg g^{-1}). The intervals of each factor and randomized run order are shown in Table 1.

The q response was calculated using the following equation:

$$q = \frac{\left(C_i - C_e\right)}{M} \times V \tag{1}$$

where q is the amount of adsorbate adsorbed in the solid phase (mg g^{-1}), C_i the initial adsorbate concentration (mg L^{-1}), C_e the final adsorbate concentration (mg L^{-1}), M adsorbent mass (g) and V solution volume (L).

The mathematical ratios between the factors and response were established by fitting the experimental data to a second-degree polynomial equation, as follows:

$$Y = \beta_0 + \sum_{i=1}^{k} \beta_i X_i + \sum_{i=1}^{k} \beta_{ii} X_i^2 + \sum_{i=1}^{k} \sum_{j=1}^{k} \beta_{ij} X_i X_j + \varepsilon \tag{2}$$

where Y is the predicted response (mg g^{-1}), X_i are the individual factors and X_i^2 the quadratic effects, $X_i X_j$ the interaction between factors, β the linear, quadratic and interactive effects and ε the randomization error.

The significance of the model developed and of each term was assessed by analysis of variance (ANOVA) based

Table 1
Data matrix

Factors	Levels				
	–2	–1	0	+1	+2
DS_C (mg L^{-1})	50	150	250	350	450
ADS_C (g L^{-1})	0.2	1.4	2.6	3.8	5
C_t (min)	5	15	25	35	45
pH	5	6	7	8	9
Run	Factors				
	DS_C (mg L^{-1})	ADS_C (g L^{-1})	C_t (min)	pH	
1	250	2.6	25	7	
2	150	1.4	15	8	
3	450	2.6	25	7	
4	350	1.4	15	6	
5	250	2.6	25	9	
6	150	3.8	35	6	
7	350	1.4	35	6	
8	250	0.2	25	7	
9	250	2.6	25	7	
10	350	1.4	15	8	
11	250	5.0	25	7	
12	150	3.8	15	8	
13	350	3.8	35	6	
14	250	2.6	25	5	
15	250	2.6	25	7	
16	150	1.4	35	6	
17	250	2.6	25	7	
18	150	3.8	15	6	
19	150	1.4	15	6	
20	250	2.6	5	7	
21	350	1.4	35	8	
22	350	3.8	15	8	
23	250	2.6	25	7	
24	350	3.8	35	8	
25	150	3.8	35	8	
26	250	2.6	45	7	
27	250	2.6	25	7	
28	350	3.8	15	6	
29	50	2.6	25	7	
30	150	1.4	35	8	

DS_C – diclofenac sodium concentration; ADS_C – adsorbent concentration; C_t – contact time; pH – potential of hydrogen.

on the probability value (p-value) and Fisher's test (F-value) at a confidence level of $p < 0.05$. The precision and predictability of the model were measured using the lack of fit criterion, coefficient of correlation (R^2), adjusted R^2, predicted R^2, adequate precision and residual normalization.

2.3.3. Kinetics and adsorption isotherms

The experimental data were fit to the kinetic models and adsorption isotherms using non-linear regression.

2.3.3.1. Kinetic models

The pseudo-first-order model assumes that the reaction is reversible, and equilibrium is established between the solid and liquid phase of the solution [39], Eq. (3).

$$q_t = q_e\left(1 - e^{-k_1 t}\right) \tag{3}$$

where q_t is the amount of adsorbate adsorbed in time t (mg g^{-1}), q_e the amount of adsorbate adsorbed in equilibrium (mg g^{-1}), k_1 the pseudo-first-order rate/speed (min^{-1}), and t the contact time (min).

The pseudo-second-order model states that the rate-limiting step is chemisorption [40], Eq. (4).

$$q_t = \frac{q_e^2 k_2 t}{1 + q_e k_2 t} \tag{4}$$

where k_2 is the pseudo-second-order rate/speed (g mg^{-1} min^{-1}).

The intraparticle diffusion model establishes that the intercept C_d is equal to zero, intra-pore adsorption plays a decisive role in the process and adsorption varies according to the square root of time [41], Eq. (5).

$$q_t = k_i t^{1/2} + C_d \tag{5}$$

where k_i is the intraparticle diffusion rate (mol g^{-1} $min^{-1/2}$) and C_d the intercept value on the q_t axis in intraparticle diffusion kinetics (mg g^{-1}).

2.3.3.2. Isotherm models

The Langmuir model is based on the formation of a single adsorption layer and assumes that adsorption sites have equal energy and are finite, meaning that adsorption peaks when the layer is formed [42], Eq. (6).

$$q_e = \frac{q_{\max} K_L C_e}{1 + K_L C_e} \tag{6}$$

where q_e is the amount of adsorbate adsorbed in equilibrium (mg g^{-1}), q_{max} the maximum amount of adsorbate adsorbed (mg g^{-1}), K_L the Langmuir adsorption constant (L mg^{-1}), and C_e adsorbate concentration at equilibrium (mg L^{-1}).

The Freundlich model assumes that adsorption sites have different energies and that the amount adsorbed never peaks due to interactions between adsorbed molecules and heterogeneous surfaces. The closer the value n is to 1, the more favorable the process [43], Eq. (7).

$$q_e = K_F C_e^{1/n} \tag{7}$$

where K_F is the Freundlich constant (mg^n $g^{-1/n}$ L^n $mg^{-1/n}$) and n the correction factor.

The models obtained will be evaluated using the coefficient of determination (R^2) and chi-squared test (χ^2).

2.3.4. Confirmation runs

The data optimized by function d_i were fit using SRM based on the following search criteria: maximum DS_C, minimum ADS_C, minimum pH and varying contact time

within the ranges tested. These data were confirmed by new adsorption assays performed in duplicate. The responses obtained in the confirmation runs were compared with those of the two-sided student's *t*-test determined at a confidence interval of $p < 0.05$.

2.3.5. Assessment of diclofenac sodium removal

The results of q were interpreted as % removal using Eq. (8).

$$\%\text{Removal} = \frac{C_e}{C_i} \times 100 \tag{8}$$

where C_e is the amount of adsorbate adsorbed in the solid phase (mg g^{-1}) and C_i the initial adsorbate concentration (mg L^{-1}).

Database searches were conducted for total removal (100%) of DS in solution at concentrations of 50, 100, 150, 200, 250, 300, 350, 400 and 450 mg L^{-1} and the respective necessary GO concentrations. The results were compiled and converted into adsorbent/adsorbate dose (g mg^{-1}). Finally, the dose needed for total DS removal was modeled by linear regression and analyzed using ANOVA, Pearson's r and the coefficient of determination.

3. Results and discussion

3.1. Graphene oxide characterization

3.1.1. X-ray diffraction

The diffractograms obtained for graphite and GO are shown in Fig. 1, with high-intensity peaks at 0 0 2 and 2θ = 10.64° (0 0 1), respectively. This difference is due to the oxidative process and insertion of functional groups such as hydroxyl, epoxy and carboxyl between GO sheets, particularly in the basal planes of the sheets during synthesis. This behavior results in wider peaks and the emergence of interplanar spacing in the direction of d002, characteristic of GO synthesis from graphite via a chemical pathway. Additionally, low-intensity peaks were observed in the 2θ = 26° region, related to the presence of impurities in the graphite [44,45].

3.1.2. Fourier-transform infrared spectroscopy with attenuated total reflectance

The Fourier-transform infrared spectroscopy with attenuated total reflectance spectra of the materials are shown in Fig. 2. The absorption spectra show similar bands for graphite powder (GP) and GO between 3,550 and 3,200 cm^{-1}, corresponding to the hydroxyl group. However, chemical oxidation deepened the peak in the corresponding region, confirming the incorporation of oxygen into structure and increased O–H concentration. Wave numbers between 3,000 and 2,840 cm^{-1} are associated with sp3-hybridized C–H bonds. The presence of CO_2 was confirmed by bands at 2,400 and 2,300 cm^{-1}. GO contains carboxyl groups at 1,720 cm^{-1} attributed to C=O bonding, epoxy groups at 1,377 and 1,029 cm^{-1} related to CO bonding, and aromatic rings at 1,616 and 702 cm^{-1} corresponding to C=C and CH bonding, respectively [46]. Thus, both XRD and FTI-ATR analysis confirmed that GO can be obtained using a modified Hummer's method. Raman, HRTEM and SEM-FEG characterizations were performed to ensure better GO analysis.

3.1.3. Raman, HRTEM and SEM-FEG

Fig. 3 shows the Raman spectrum obtained for GO and used to study DS adsorption, with peaks at bands D

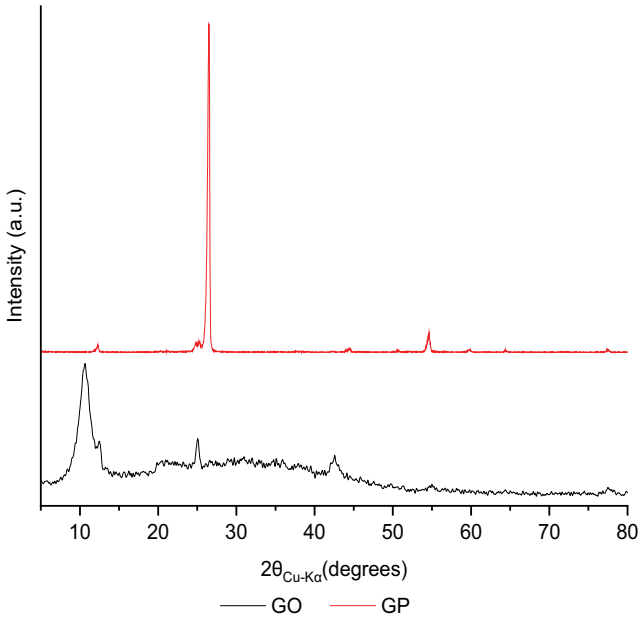

Fig. 1. X-ray diffractions for graphite powder (GP) and graphene oxide (GO).

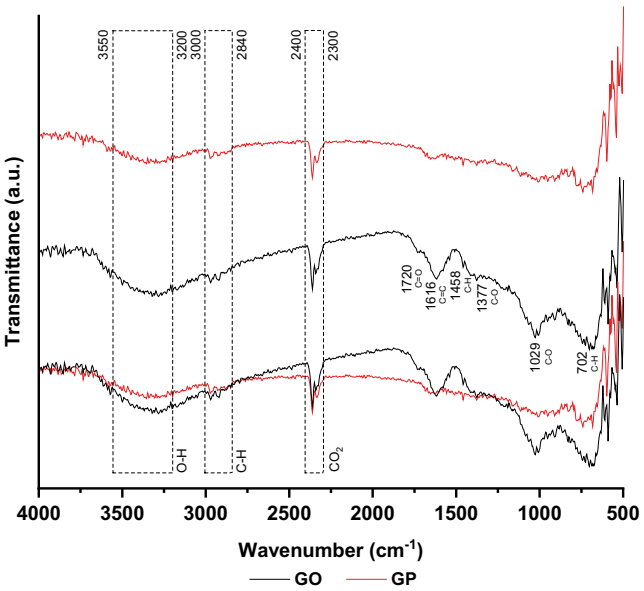

Fig. 2. Fourier-transform infrared spectroscopy with attenuated total reflectance of graphite powder (GP) and graphene oxide (GO).

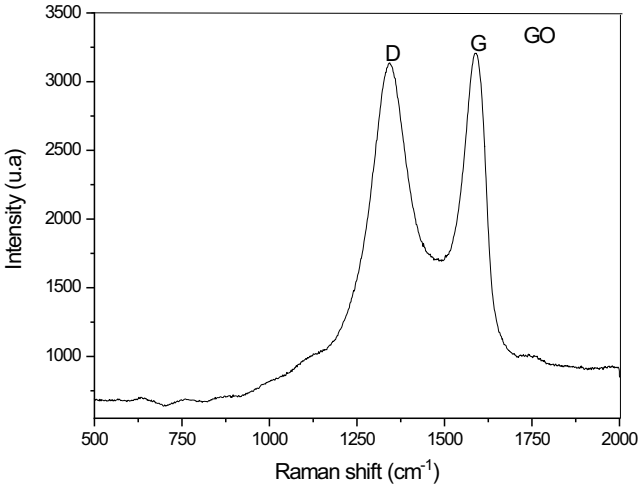

Fig. 3. Raman spectroscopy of graphene oxide (GO).

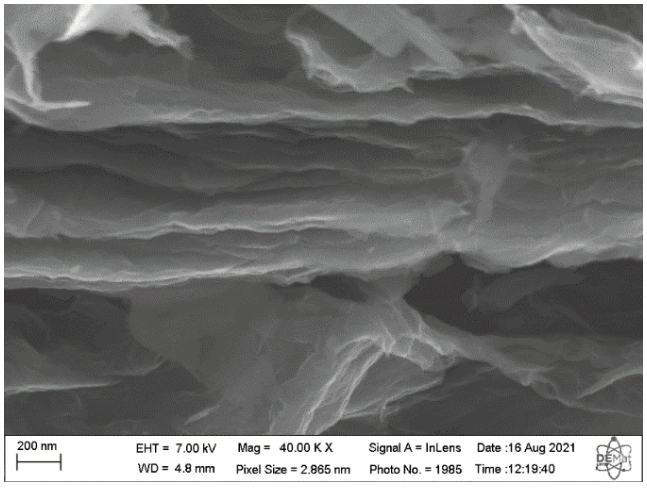

Fig. 4. SEM-FEG of graphene oxide (GO) samples at 40,000× magnification.

(~1,345 cm^{-1}) and G (~1,587 cm^{-1}). The G band is attributed to first-order scattering of E2g phonons by sp^2-bonded carbon and the D band to defects associated with vacancies and grain boundaries. The D to G band intensity ratio makes it possible to determine the number of defects present in the carbon structure, with a value of approximately 0.86 for the GO obtained via synthesis. The same values were also reported by Kim et al. [47].

Microstructural assessment of GO obtained by SEM-FEG is illustrated in Fig. 4. The image shows a microstructure composed of several wrinkled, folded layers, with the wrinkling attributed to the oxidation that occurs during synthesis, enabling the entry of hydroxyl and epoxy groups and transforming the hybridized sp^2 carbons (planar geometry) of graphite into GO sp^3 carbons (tetrahedral geometry). The formation of these oxygen-bearing functional groups in the basal planes causes structural defects in GO and the greater the degree of oxidation, the larger the spaces between the layers. Although GO obtained from graphite via chemical oxidation generally exhibits a relatively good yield, these spaces/defects typically lead to the formation of irregular defective structures when compared to the bottom-up method, which is based on graphene formation from gases with a high carbon concentration, as occurs in CVD (chemical vapor deposition) [48,49].

Fig. 5a shows an HRTEM image that confirms the presence of sheets. The GO material shows a good level of transparency, indicating a high degree of graphite powder exfoliation. The dark regions are related to the stacked layers of GO, which also displays an amorphous unorganized morphology [50]. The scattered area electron diffraction (SAED) pattern of GO (Fig. 5b) shows only diffraction rings and the diffraction points are not defined, confirming that the GO sheets are amorphous. This finding is corroborated by XRD analysis. The electron diffraction rings obtained by SAED show an interplanar distance *d* of approximately 1.2 Å and 2.1 Å corresponding to *d* in graphene and suggesting the presence of graphitic regions within graphene oxide [51].

3.1.4. Point of zero charge

The point of zero charge (PZC) is the pH at which the net charge on the surface of the adsorbent is zero, that is, the surface has the same affinity for anions and cations. When solution pH is above the PZC, the surface of the material is negatively charged and shows greater affinity for cations, becoming positively charged with higher anion affinity when pH falls below zero.

The PZC obtained for GO was 1.65 (Fig. 6), demonstrating acidity according to the FTI-ATR results and the predominance of carboxyls over hydroxyls in GO. Additionally, GO remained ionized under all the pH conditions in the batch tests (PZC_{GO} 1.65 < $pH_{solution}$ 5 – 9).

3.1.5. Brunauer–Emmett–Teller

Nitrogen adsorption onto GO and GP is shown in Fig. 7 and its parameters in Table 2. Chemical oxidation was effective and increased the surface area by around 255.92%. The BET method estimated the surface area of GP and GO at 45.92 and 117.58 $m^2\ g^{-1}$, respectively. Although the values obtained in the present study partially corroborate those reported in the literature of 70–1,000 $m^2\ g^{-1}$ for synthesized GO, several studies argue that GO is not sufficiently porous to adsorb nitrogen and/or that residual reagents (acids) interfere in the outcome, and/or the water present in the sample acts as a solvent for nitrogen until saturation is reached, preventing contact with the GO surface for adsorption and resulting in surfaces that do not reflect reality [52–54].

3.2. Batch adsorption study

3.2.1. Adsorption capacity response (q)

The data predicted by the model developed for GO are satisfactory in relation to actual data, with the residual model varying from approximately 0.02 to 40.62 mg g^{-1} (Table 3) and homogeneous distribution for actual vs. predicted data, as shown in Fig. 8.

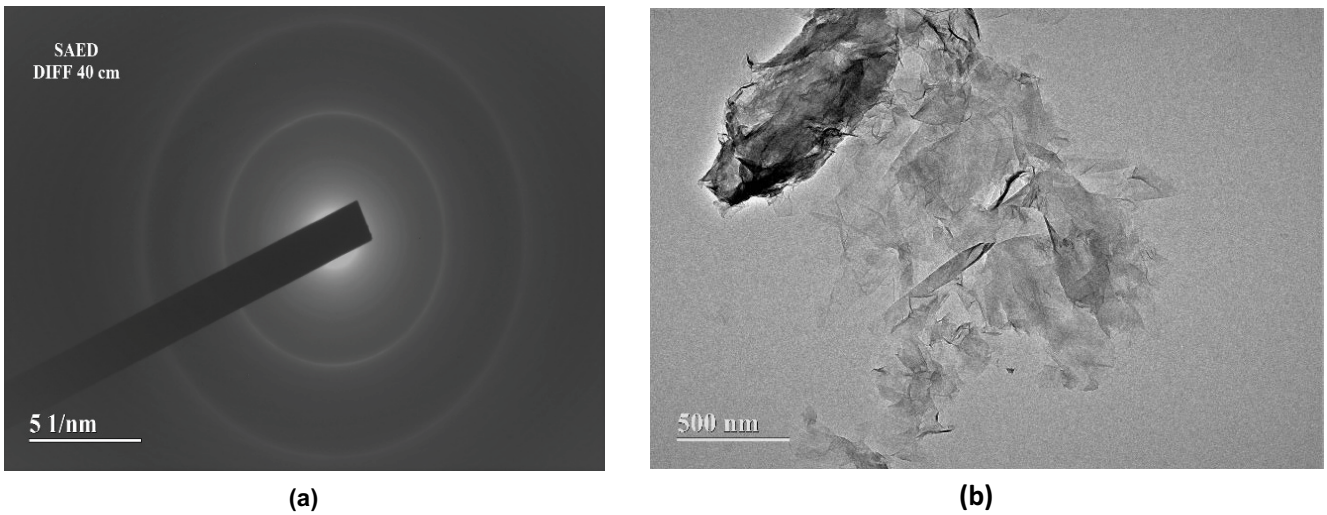

Fig. 5. (a) High-resolution microscopy and (b) scattered area electron diffraction of the graphene oxide (GO) sample.

Table 2
BET summary

Material	Slope	Intercept	*r*	*C*	S_{BET} ($m^2\ g^{-1}$)
GP	59.50	1.64E+01	0.9981	4.64	45.92
GO	19.61	1.00E+01	0.9945	2.96	117.58

r – Pearson's *r*; *C* –; S_{BET} – specific surface area; GP – graphite powder; GO – graphene oxide.

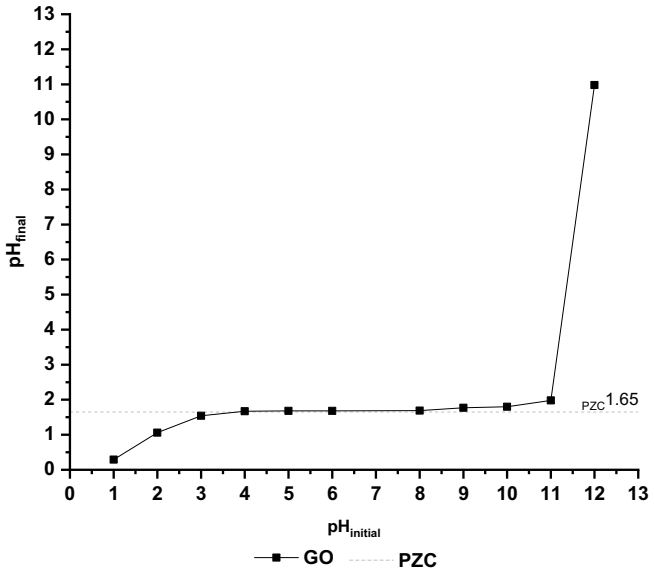

Fig. 6. Point of zero charge (PZC) determination for graphene oxide (GO).

The experimental data (q_{actual}), responses predicted by the model ($q_{predicted}$) and their respective residuals are presented in Table 3.

The real and actual data were analyzed using the lack-of-fit test, with an *F*-value of 6080.10 and significance (*p*-value) < 0.0001 for GO, indicating the presence of outliers and nonlinear unbalanced actual values (Fig. 8, Table 4). There was a difference between actual and predicted *q* values in runs 8 and 11, with a smaller (0.2 g L^{-1}) and larger (5.0 g L^{-1}) amount of adsorbent, respectively.

The coefficient of determination (R^2) obtained by multiple linear regression was 0.9910, considered satisfactory to validate the model used. The adjusted R^2 for oxide was 0.9827, close to the predicted value of 0.9484, indicating that the model can be used to describe DS adsorption by GO with no mathematical reduction, considering a predicted $R^2 < 20\%$ of the adjusted R^2 [55].

The model developed for response *q* was submitted to analysis of variance (ANOVA), with the results presented in Table 4. In general, $p < 0.05$ indicates statistical significance for a 95% confidence interval. Based on this reference, the data demonstrate that the model is statistically significant, with $p < 0.0001$. Individual factorial analysis suggests significance for $DS_C \cdot ADS_C \cdot DS_C \cdot ADS_C \cdot DS_C^2 \cdot ADS_C^2$ for the values tested.

Using the maximum coefficient of variation (CV) of 10% as a relative measure to valid repeatability, the model for *q* was adequate, with a CV of 4.40% [56]. In terms of precision, values greater than 4 are considered adequate [56], indicating a better signal-to-noise ratio response. Model precision was deemed satisfactory at 46.62. The *F*-value of 118.41 corroborates model validation, with $p < 0.0001$.

3.2.2. Perturbation analysis

The influence of adsorbate concentration, adsorbent mass, contact time and pH in relation to the central point in the experimental models is shown in Fig. 9.

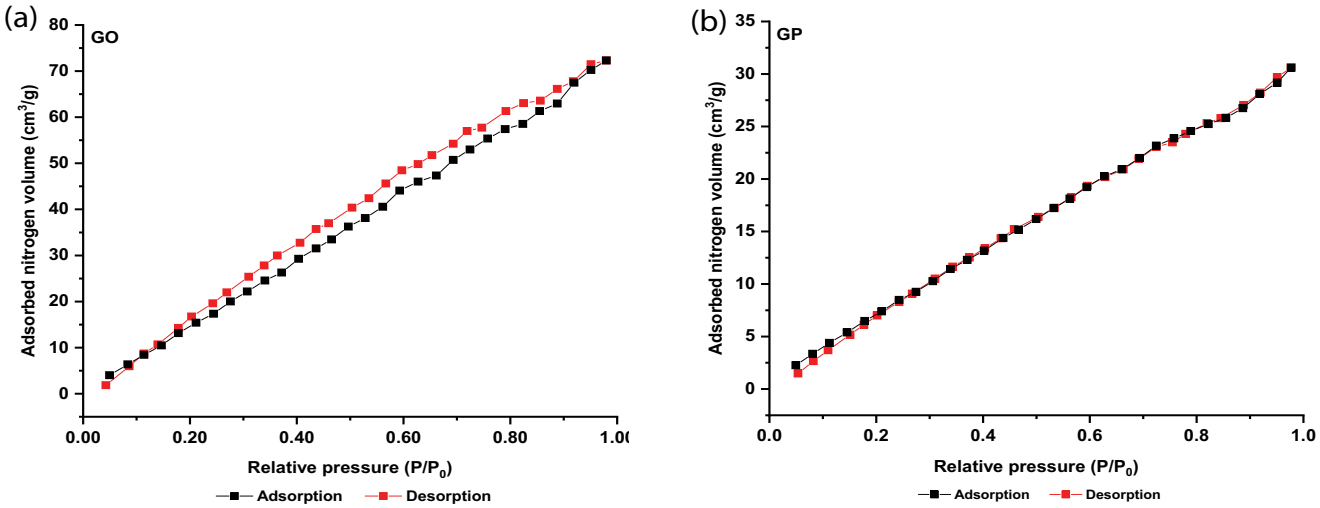

Fig. 7. Nitrogen adsorption onto (a) graphene oxide (GO) and (b) graphite powder (GP).

Table 3
Data matrix, experimental data, predicted data and residuals

Run	*A*	*B*	*C*	*D*	q_{actual}	$q_{predicted}$	*R*	*R*%
1	250	2.6	25	7	95.30	95.27	0.03	99.12
2	150	1.4	15	8	104.86	110.26	–5.40	97.87
3	450	2.6	25	7	172.60	172.52	0.08	99.73
4	350	1.4	15	6	248.42	256.75	–8.33	99.37
5	250	2.6	25	9	94.78	94.66	0.12	98.57
6	150	3.8	35	6	39.31	36.36	2.95	99.59
7	350	1.4	35	6	249.74	257.74	–8.00	99.90
8	250	0.2	25	7	412.89	372.27	40.62	33.03
9	250	2.6	25	7	95.26	95.27	–0.02	99.07
10	350	1.4	15	8	247.98	255.80	–7.82	99.19
11	250	5.0	25	7	49.75	64.93	–15.17	99.51
12	150	3.8	15	8	38.70	35.71	2.99	98.03
13	350	3.8	35	6	91.91	87.27	4.64	99.79
14	250	2.6	25	5	95.68	95.38	0.30	99.51
15	250	2.6	25	7	95.11	95.27	–0.16	98.92
16	150	1.4	35	6	106.09	111.68	–5.60	99.02
17	250	2.6	25	7	95.11	95.27	–0.16	98.92
18	150	3.8	15	6	38.89	35.79	3.10	98.53
19	150	1.4	15	6	105.30	110.68	–5.39	98.28
20	250	2.6	5	7	93.84	93.79	0.04	97.59
21	350	1.4	35	8	248.24	256.79	–8.54	99.30
22	350	3.8	15	8	91.17	86.40	4.77	98.98
23	250	2.6	25	7	95.44	95.27	0.17	99.26
24	350	3.8	35	8	91.75	86.97	4.78	99.61
25	150	3.8	35	8	39.31	36.28	3.04	99.59
26	250	2.6	45	7	95.68	95.31	0.37	99.95
27	250	2.6	25	7	95.40	95.27	0.13	99.21
28	350	3.8	15	6	91.43	86.71	4.72	99.26
29	50	2.6	25	7	18.90	18.74	0.16	98.28
30	150	1.4	35	8	105.91	111.25	–5.34	98.85

A – diclofenac sodium concentration; *B* – adsorbent concentration; *C* – contact time; *D* – pH; q_{actual} – actual adsorption capacity (mg g^{-1}); $q_{predicted}$ – predicted adsorption capacity (mg g^{-1}); *R* – residue; *R*% – removal rate.

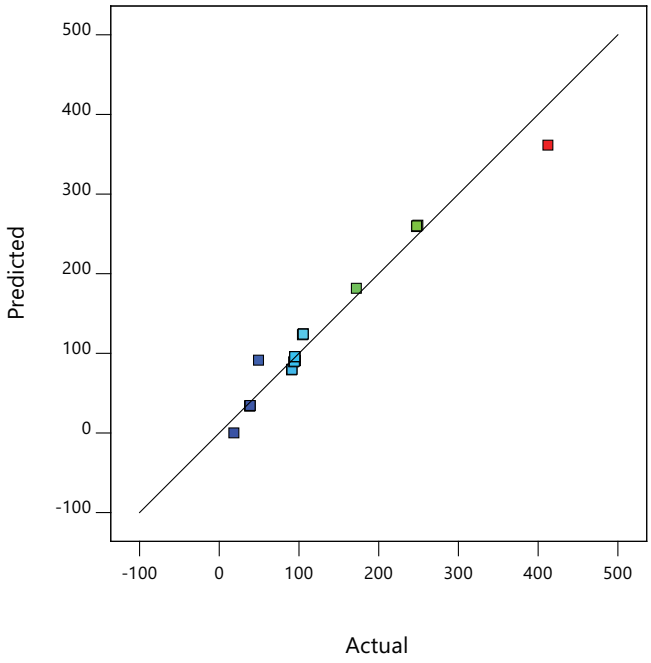

Fig. 8. Predicted vs. actual adsorption capacity for graphene oxide (GO).

As indicated by ANOVA, adsorbate concentration and adsorbent mass influenced the response, with steep slopes indicating that q is highly sensitive to these factors. By contrast, pH and contact time did not significantly affect the efficiency of the process, DS_C and C_t are considered synergistic factors and ADS_C are pH antagonist.

3.2.3. Response surfaces for diclofenac sodium absorption onto graphene oxide

Response surfaces (RS) for DS absorption capacity onto GO are presented in Fig. 10.

Adsorption capacity increased at SD and GO concentrations above 350 mg L^{-1} and 1.4 g L^{-1}, respectively, contact time >25 min and pH < 6. However, ANOVA, perturbation analysis and the 3D graph demonstrated that pH and contact time did not significantly influence adsorption.

By contrast, a lower adsorbent dose increased adsorption capacity, exhibiting greater efficiency in the region below 1.4 g L^{-1}, converging with 0.2 g L^{-1} (Fig. 10a). This antagonistic effect is likely due to the fact that low concentrations of powdered absorbents disperse more homogeneously in the liquid column and do not aggregate [57].

Longer contact times resulted in increased adsorption capacity, which can be explained by structural arrangement of GO in stacked layers (Fig. 10b and f). Under

Table 4
ANOVA for the adsorption capacity of diclofenac sodium (DS) onto graphene oxide (GO)

Source	df	Sum of squares	Mean square	*F*-value	*p*-value
Model	14	341.61	24.40	118.41	<0.0001
DS_C	1	116.31	116.31	564.41	<0.0001
ADS_C	1	189.40	189.40	919.07	<0.0001
C_t	1	0.0091	0.0091	0.0443	0.8362
pH	1	0.0020	0.0020	0.0099	0.9222
$DS_C \cdot ADS_C$	1	4.73	4.73	22.93	0.0002
$DS_C \cdot C_t$	1	0.0003	0.0003	0.0013	0.9712
$DS_C \cdot pH$	1	0.0001	0.0001	0.0004	0.9837
$ADS_C \cdot C_t$	1	9.338E-08	9.338E-08	4.531E-07	0.9995
$ADS_C.pH$	1	0.0002	0.0002	0.0009	0.9768
$C_t \cdot pH$	1	2.626E-09	2.626E-09	1.274E-08	0.9999
DS_C^2	1	1.81	1.81	8.80	0.0096
ADS_C^2	1	26.28	26.28	127.52	<0.0001
C_t^2	1	0.0024	0.0024	0.0114	0.9163
pH^2	1	0.0003	0.0003	0.0013	0.9712
Residual	15	3.09	0.2061		
Lack of fit	10	3.09	0.3091	6,080.10	<0.0001
Pure error	5	0.0003	0.0001		
Cor. total	29	344.68			

Fit statistics			R^2	0.9910
	Std. dev.	0.4540	Adjusted R^2	0.9827
	Mean	10.33	Predicted R^2	0.9484
	C.V.%	4.40	Adeq. precision	46.6216

DS_C – diclofenac sodium concentration; ADS_C – adsorbent concentration; C_t – contact time; pH – potential of hydrogen.

these conditions, a longer contact time may favor internal diffusion between the layers and optimize adsorption [58]. In regard to pH, the acid medium (pH < 7) may have favored the desolubilization of DS, whose pKa of 4.15 causes the adsorbate to precipitate on the surface of the adsorbent composed of oxygenated functional groups. Fig. 10c [37]. DS ($pH_{solution}$ 5–9 > DS_{pKa} 4.15) and GO ($pH_{solution}$ 5–9 > PZC_{GO} 1.65) were ionized at all the pH tested, demonstrating adsorbate–adsorbent repulsion in the liquid, meaningthat SD adsorption onto GO is not explained by electrostatic mechanisms [59], but rather π-π bonds, hydrogen bonds and van der Waals forces, as observed in other studies [45,60].

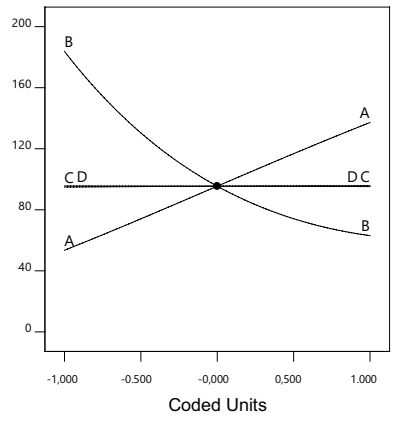

A – diclofenac sodium concentration; B – adsorbent concentration; C – contact time; D – pH.

Fig. 9. Perturbation plot.

3.2.4. Optimizing diclofenac sodium adsorption onto graphene oxide and confirmation runs

The results of maximum adsorption capacity and experimental confirmation runs are presented in Table 5.

The maximum adsorption capacity obtained for the model was 618.81 mg g^{-1}, corresponding to d_i = 1.00. In order to reproduce this result, a combination of factors was tested in duplicate, resulting in an average capacity of 669.50 mg g^{-1}, 8.19% higher than that predicted by the model.

3.2.5. Kinetic models

The adsorption kinetics for different DS concentrations on GO are shown in Fig. 11.

Fig. 11 indicates that adsorption capacity (q) remains stable over time for all the concentrations tested. As such, there is evidence that DS adsorption onto GO occurs instantaneously, as observed in other adsorption studies with different micropollutants, such as aspirin – analgesic, caffeine – thermogenic, acetaminophen – paracetamol, tetracycline – antibiotic and methylene blue – organic dye [34,58,61]. The goodness of fit of the kinetic models to the data demonstrated that the pseudo-second-order model exhibited a better fit to the kinetics of DS adsorption onto

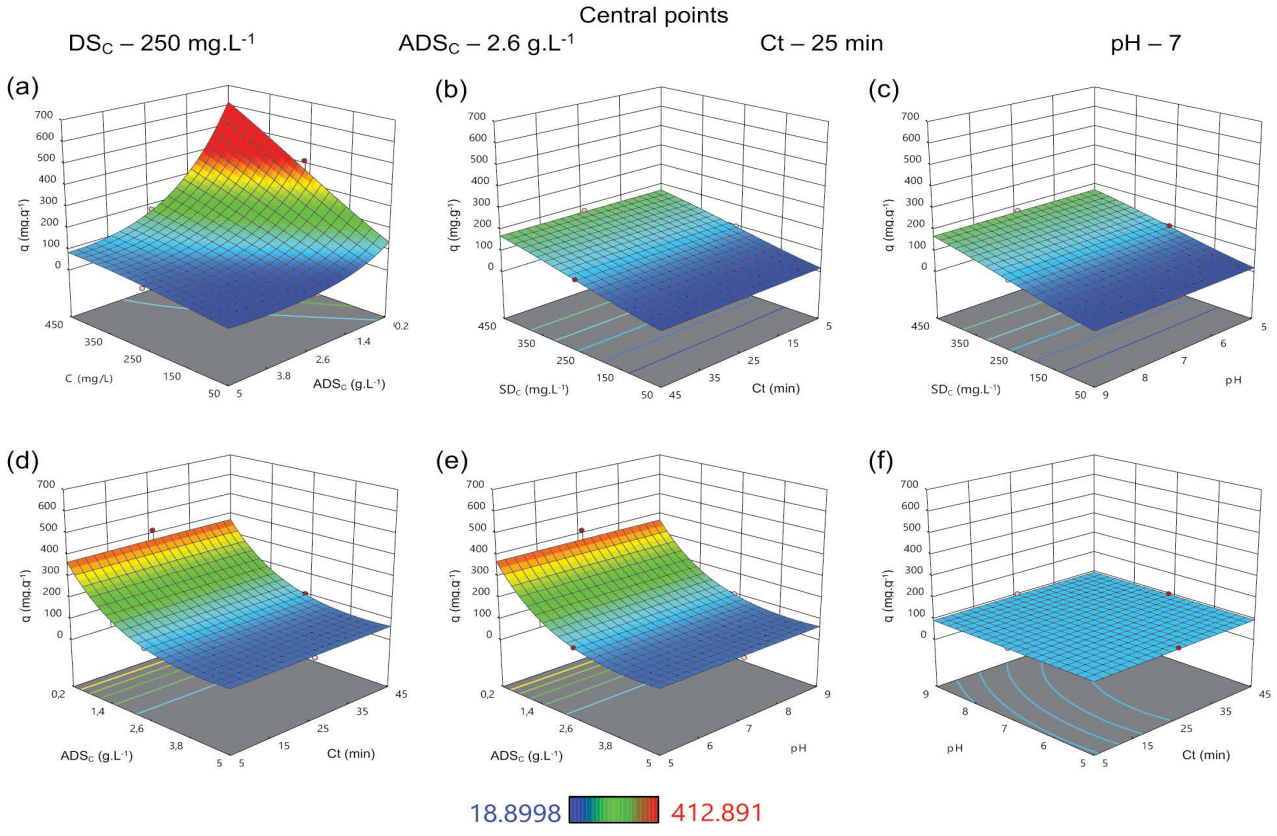

Fig. 10. Response surfaces for diclofenac sodium (DS) adsorption capacity onto graphene oxide (GO).

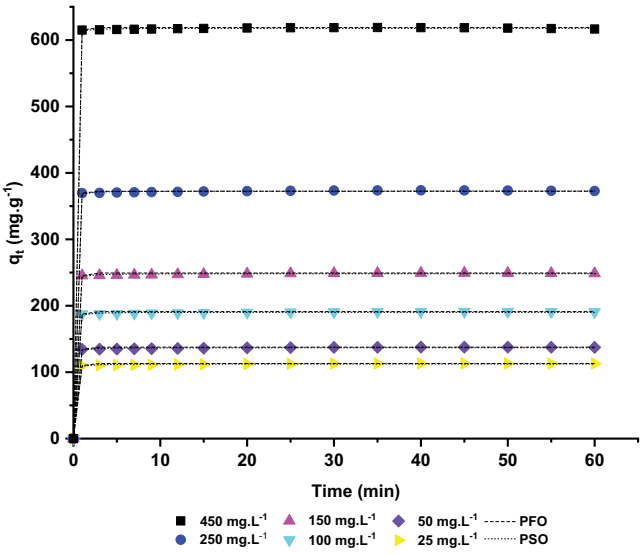

Fig. 11. Comparison of experimental data with pseudo-first-order and pseudo-second-order kinetic models.

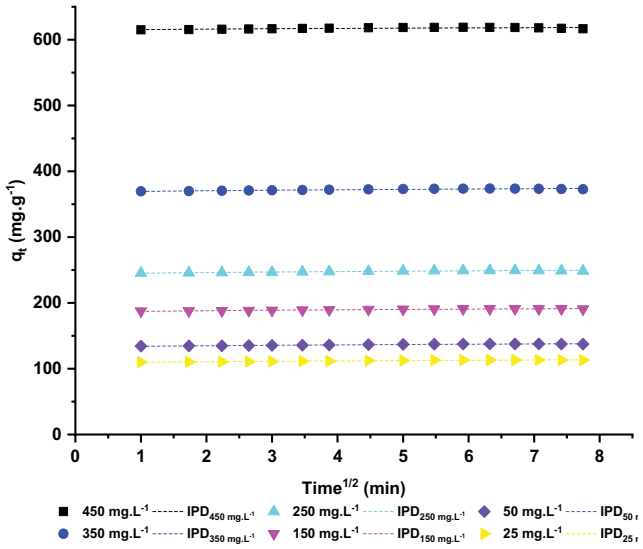

Fig. 12. Comparison of experimental data with pseudo-first-order and pseudo-second-order kinetic models.

Table 5
Maximum adsorption capacity, factor levels and confirmation runs

Factors	Conditions
DS_C	450 mg L^{-1}
ADS_C	0.2 g L^{-1}
C_t	34.3 min
pH	5
q_{max}	618.81 mg g^{-1}
d_i	1.00
Confirmation runs	
q_1	671.64 mg g^{-1}
q_2	667.35 mg g^{-1}
Student's *t*-test	
$Limit_{low}$	504.79 mg g^{-1}
q_{mean}	669.50 mg g^{-1}
$Limit_{upp}$	743.97 mg g^{-1}

DS_C – diclofenac sodium concentration; ADS_C – adsorbent concentration; C_t – contact time; q_{max} – maximum adsorption capacity; d_i – Derringers desirability; $Limit_{low}$ – lower limit; $Limit_{upp}$ – upper limit; q_{mean} – mean of runs.

GO, since it obtained a lower χ^2 and higher R^2 in relation to the other conditions tested, as shown in Table 6. For pseudo-first-order, the adsorption rate represented by k_1 and the R^2 value increased as the DS concentration rose, as observed by Azizian [62]. The k_2 rate of the pseudo-second-order model varied at the levels tested, but its higher R^2 values in relation to the pseudo-first-order model indicated greater adaptation, since pseudo-second-order is based on an empirical model [40].

In order to investigate the adsorption mechanisms, the intraparticle diffusion model was also fit to the adsorption data of different DS concentrations on GO, with the results displayed in Fig. 12.

The adjustment parameters for the intraparticle diffusion model revealed that more than one mechanism (intraparticle and intrafilm diffusion) controls the adsorption process, since the straight line does not intercept the origin in the q_t vs. $t^{1/2}$ graph, as shown in Fig. 12 [41,63]. However, the C_d and q_e values are very similar (Table 6. pseudo-first-order) and indicate that 98.19% to 99.16% of DS was adsorbed onto the GO surface via intrafilm diffusion, meaning that this mechanism predominates, which, when combined with the physical and chemical characteristics of GO and adsorption characteristics of DS, demonstrates the occurrence of chemisorption [41,64].

3.2.6. Equilibrium isotherms

Fig. 13 shows the equilibrium isotherms for DS adsorption onto GO.

The linear-concave shape of the isotherm shows a constant partition between the solute and solution and does not indicate maximum adsorption capacity [65]. The GO data exhibited a satisfactory fit to both models, with R_L and $1/n < 1$, indicating an excellent adsorbate–adsorbent ratio and low liquid-adsorbate ratio [42]. The equilibrium ratio is best described by the Freundlich model with $R^2 = 0.9913$ and low χ^2. The Freundlich model is based on surface heterogeneity and assumes an unlimited number of active sites [43]. Thus, the equation is consistent with the linear shape of the isotherm, with no maximum absolute adsorption capacity.

The Langmuir q_{max} value for maximum adsorption capacity was 1,704.94 mg g^{-1}, far higher than those of 618.81 mg g^{-1} (model) and 669.50 mg g^{-1} (confirmation run), Table 5 and 7. Separation factor R_L in this isotherm indicates that the greater the initial concentration, the better the affinity between DS and GO, since the value is greater than 1 (Table 7). In the Freundlich isotherm, the value of $1/n$ is close to 1, denoting a

Table 6
Kinetic model parameters for different concentrations

Models	25 mg L^{-1}	50 mg L^{-1}	100 mg L^{-1}	150 mg L^{-1}	250 mg L^{-1}	450 mg L^{-1}
Pseudo-first-order						
q_e (mg g^{-1})	112.99	137.67	191.14	249.29	373.71	618.80
k_1 (L mg^{-1})	3.6553	3.7172	3.9465	4.1479	4.4954	5.0749
χ^2	1.6628	2.3059	2.7444	3.0460	3.2715	2.8836
R^2	0.9978	0.9979	0.9987	0.9992	0.9996	0.9999
Pseudo-second-order						
q_e (mg g^{-1})	112.44	136.87	190.27	248.38	372.74	617.78
k_2 (L g^{-1})	0.2990	0.2808	0.2560	0.2415	0.2320	0.2747
χ^2	0.6551	0.7374	0.8693	0.9521	0.9792	0.8066
R^2	0.9992	0.9993	0.9995	0.9998	0.9999	1.0000
Intraparticle diffusion						
K_d (mol g^{-1} $min^{-1/2}$)	2.0505	2.1794	2.3731	2.4859	2.4913	1.7771
C_d (mg g^{-1})	107.71	131.84	184.79	242.62	366.95	613.57
χ^2	0.0566	0.0703	0.1037	0.1466	0.2698	0.7179
R^2	0.9559	0.9517	0.9406	0.9246	0.8695	0.5496

q_e – amount of adsorbate adsorbed in equilibrium; k_1 – pseudo-first-order rate/speed (min^{-1}); k_2 – pseudo-second-order rate/speed (g mg^{-1} min^{-1}); K_d – diffusion rate (mol g^{-1} $min^{-1/2}$); C_d – value of the intersection with the q_t axis in intraparticle diffusion kinetics (mg g^{-1}); χ^2 – chi-squared; R^2 – coefficient of determination.

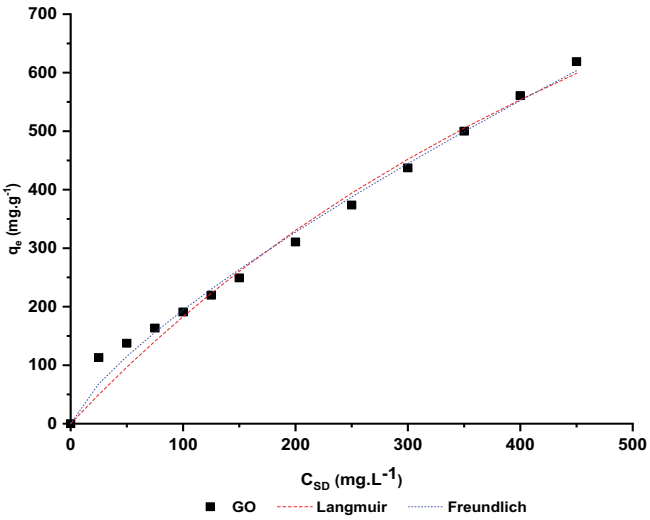

Fig. 13. Comparison of experimental data with Langmuir and Freundlich models.

linear mode [43] and corroborating our observations, which, when combined with the absence of an absorption resistance curve for DS onto GO, demonstrate greater adsorption capacities than those recorded here can be achieved at concentrations >450 mg g^{-1}.

3.2.7. Comparison of adsorption capacity with the literature

The maximum adsorption capacity obtained for GO in the present study and that of different materials found in the literature are presented in Table 8.

Table 7
Isotherm model parameters for equilibrium capacity

Models	
Langmuir	
q_{max} (mg g^{-1})	1,704.94
K_L (L mg^{-1})	0.0012
R_L (25 mg L^{-1})	0.9709
R_L (450 mg L^{-1})	0.6494
χ^2	716.90
R^2	0.9814
Freundlich	
K_F (mg^n $g^{-1/n}$ L^n $mg^{-1/n}$)	6.0294
n	1.3263
$1/n$	0.7540
χ^2	337.58
R^2	0.9913

q_{max} – maximum amount of adsorbate adsorbed (mg g^{-1}); K_L – Langmuir adsorption constant (L mg^{-1}); K_F – Freundlich constant (mg^n $g^{-1/n}$ L^n $mg^{-1/n}$); $1/n$ – constant associated with surface heterogeneity; χ^2 – chi-squared; R^2 – coefficient of determination.

As shown in Table 8, GO is among the materials with the highest adsorption capacity and its adsorbate–adsorbent ratio (g mg^{-1}) of 0.0004 is among the three lowest, similar to the results for reduced graphene oxide (RGO), with 0.0003 and maximum capacity of 59.67 mg g^{-1}, and those of porous graphitic biochar (PGB) at 0.0005 and 123.45 mg g^{-1}. This demonstrates that these materials may exhibit better

Table 8
Comparison of maximum diclofenac sodium adsorption capacity onto different adsorbents reported in the literature

Adsorbent	q_{max} (mg g^{-1})	DS_C (mg L^{-1})	ADS_C (g L^{-1})	Dose (g mg^{-1})	T_c (min)	pH	Reference
Cocoa pod husks	5.53	30	5	0.1667	45	7	[67]
Reduced graphene oxide	59.67	200	0.6	0.0003	200	10	[68]
Porous graphitic biochar	123.45	20	0.1	0.0005	1440	6.5	[69]
Cationic polymeric nanoparticles	334.20	500	1.2	0.0024	7	7	[70]
Porous polyethyleneimine microspheres	572.67	1000	1.5	0.0015	242	5	[71]
Our study	669.50	450	0.2	0.0004	40	5	

dispersion in the liquid column, thereby providing a larger available surface area than the other materials. In regard to contact time, RGO, PGB and porous polyethyleneimine microspheres (PPM) achieved maximum absorption capacity at longer times than those of the other materials. Although the morphology of RGO is similar to that of GO, its reduction with basic compounds resulted in its deoxygenation, that is, the loss of functional groups responsible for the absorption mechanisms observed in our study. As such, its maximum absorption capacity is lower and contact time longer than those of GO. The porous structure of PGB and PPM is the main cause of the increased contact time needed to achieve saturation, since intraparticle diffusion is secondary to intrafilm diffusion. In terms of pH, RGO is the only material that indicates the basic medium (10) as optimal, which can be explained by the fact that ionized DS is electrostatically attracted to its positively charged surface.

3.2.8. Assessment of diclofenac sodium removal by adsorption onto graphene oxide

The optimal GO doses and masses needed for total removal (100%) of different DS concentrations by adsorption are shown in Fig. 14.

The predicted 100% removal of DS from aqueous solution was obtained for all the adsorbate concentrations tested (50 to 450 mg L^{-1}). The masses and doses needed to achieve maximum removal efficiency are presented in Table 9.

Fig. 14 shows that the mass required to achieve 100% removal remains relatively stable between 200 and 400 mg L^{-1}, which may be because the higher DS concentration (increased solution saturation) acts as a "catalyst", forcing contact with the surface of the adsorbent, which promotes chemisorption. Additionally, the actual removal percentages recorded for all the adsorbate concentrations and masses between 1.4 and 5 g L^{-1} ranged from 97.59% to 99.95%, with a median of 99.15% for the dataset. The high efficiencies (close to 100%) found in the present study for GO were also reported by Al-Khateeb et al. [34] for caffeine, aspirin and paracetamol removal and Duru et al. [72] for heavy metals.

In addition to these data, linear regression and correlation of the concentrations with the adsorbent doses needed for total DS removal by adsorption onto GO in aqueous solution are presented below (Table 10). The dose-concentration ratio is negative and displays a strong linear correlation, with Pearson's r = –0.9794 and R^2 = 0.9592.

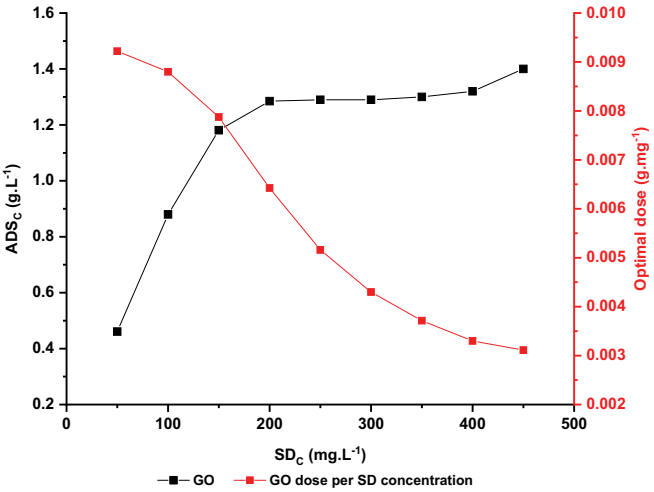

Fig. 14. Masses and doses for total diclofenac sodium (DS) removal by adsorption onto graphene oxide (GO).

The DS concentration in solution (mg L^{-1}) is input into the dose equation [Eq. (9)] to calculate the GO dose in grams needed for every milligram of DS (g mg^{-1}). This dose is then used to calculate the adsorbent concentration (g L^{-1}) to be added to the solution in order to achieve the expected 100% removal.

$$\frac{GO}{DS_{dose}} = 0.01005 - 1.71262 \times 10^{-5}.DS_C \quad (9)$$

4. Conclusions

The physical and chemical characteristics of GO (structural arrangement sheets, nanometric size, hydrophobicity, oxygenated functional groups) enable strong adsorbent–adsorbate bonds via adsorption mechanisms based on electron sharing, mainly π-π and hydrogen bonds.

The CCD used in the batch adsorption study proved to be an excellent optimization tool, demonstrating that a pH between 5 and 9 and contact time of 5 to 45 min did not significantly influence adsorption capacity for DS concentrations of 50 to 450 mg L^{-1} and 0.2 to 5 g L^{-1} of GO. Removal efficiency was close to 100% for all the concentrations tested (50 to 450 mg L^{-1}), with 0.46 and 1.38 g L of GO needed to completely remove 50 and 450 mg L^{-1} of DS in aqueous solution.

Table 9
Masses and doses for total (100%) diclofenac sodium removal by adsorption onto graphene oxide

Parameters	Diclofenac sodium (mg L^{-1})								
	50	100	150	200	250	300	350	400	450
ADS_C (g L^{-1})	0.46	0.88	1.18	1.28	0.29	1.30	1.30	1.32	1.38
GO/SD_D (g mg^{-1})	0.0092	0.0088	0.0079	0.0064	0.0052	0.0043	0.0037	0.0033	0.0031

ADS_C – adsorbent concentration; GO/SD_D – required graphene oxide dose per milligram of diclofenac sodium.

Table 10
ANOVA parameters and statistics for total (100%) diclofenac sodium removal

ANOVA					
Source of variation	df	Sum of squares	Mean square	*F*-value	*p*-value
Model	1	4.39961E-5	4.39961E-5	164.70758	4.04593E-6
Error	7	1.86981E-6	2.67116E-7		
Total	8	4.58659E-5			
Linear regression					
Source	Coefficients		Standard error	*t*-value	*p*-value
Intercept	0.01005		3.75471E-4	26.76278	2.60564E-8
Slope	–1.71262E-5		1.33446E-6	–12.83385	4.04593E-6
Model statistics	Values				
Number of points	9				
Degrees of freedom	7				
Residual sum of squares	1.86981E-6				
Pearson's *r*	–0.9794				
R^2	0.9592				
Adj. R^2	0.95341				

ANOVA – analysis of variance; R^2 – coefficient of determination; df – degrees of freedom.

The pseudo-second-order kinetic model exhibited the best fit to the data, with an R^2 value of 0.9992. The intraparticle diffusion model revealed that intrafilm diffusion predominates in the adsorption process, with around 98.19% to 99.16% of DS adsorbed on the surface. Adsorption equilibrium was best explained by the Freundlich model, with $R^2 = 0.9913$. The maximum capacity of 669.50 mg g^{-1} demonstrated that adsorption can be improved by DS concentrations greater than 450 mg L^{-1}, since the Langmuir model ($R^2 = 0.9814$) predicted a maximum of 1,704.94 mg g^{-1}.

In conclusion, GO shows excellent characteristics for application in possible advanced water treatment cells because of the short contact time needed, its ability to adapt to different pH and pollutant concentrations without yield loss and the fact that its chemisorption mechanism ensures better safety with no micropollutant desorption.

Conflicts of interest

There are no conflicts of interest to declare.

Acknowledgments

This study was partially funded by the CNPq (National Council for Scientific and Technological Development or Conselho Nacional de Pesquisa in Portuguese) under process number 426935/2018-7.

References

[1] ANVISA – Resolução da Diretoria Colegiada – RDC Nº 200, DE 26 DE DEZEMBRO DE 2017, Ministério da Saúde – MS, Agência Nacional de Vigilância Sanitária – ANVISA. Available at: http://antigo.anvisa.gov.br/documents/10181/3836387/%283%29RDC_200_2017_COMP.pdf/6316bee6-095d-426b-9398-6b1f659078b5 (Accessed April 2020).
[2] K. Kümmerer, Drugs in the environment: emission of drugs, diagnostic aids and disinfectants into wastewater by hospitals in relation to other sources--a review, Chemosphere, 45 (2001) 957–969.
[3] T.A.D. Beek, F.-A. Weber, A. Bergmann, S. Hickmann, I. Ebert, A. Hein, A. Küster, Pharmaceuticals in the environment-global occurrences and perspectives, Environ. Toxicol. Chem., 35 (2015) 823–835.
[4] S. González-Alonso, L.M. Merino, S. Esteban, M.L. de Alda, D. Barceló, J.J. Durán, J. López-Martínez, J. Aceña, S. Pérez, N. Mastroianni, A. Silva, M. Catalá, Y. Valcárcel, Occurrence of pharmaceutical, recreational and psychotropic drug residues in surface water on the northern Antarctic Peninsula region, Environ. Pollut., 229 (2017) 241–254.
[5] K.V. Thomas, K.H. Langford, Green and Sustainable Pharmacy, Springer Berlin Heidelberg, Berlin, 2010, pp. 211–223.

[6] C.I. Kosma, D.A. Lambropoulou, T.A. Albanis, Occurrence and removal of PPCPs in municipal and hospital wastewaters in Greece, J. Hazard. Mater., 179 (2010) 804–817.
[7] D. Taylor, T. Senac, Human pharmaceutical products in the environment – the "problem" in perspective, Chemosphere, 115 (2014) 95–99.
[8] D.R.S. Lima, M.D. Tonucci, M. Libânio, S.F. Aquino, Pharmaceuticals and endocrine disrupting compounds in Brazilian waters: occurrence and removal techniques, Eng. Sanit. Ambient., 2 (2017) 1043–1054.
[9] P. McGettingan, D. Henry, Use of non-steroidal anti-inflammatory drugs that elevate cardiovascular risk: an examination of sales and essential medicines lists in low-, middle-, and high-income countries, PLoS Med., 10 (2013) e1001388, doi: 10.1371/journal.pmed.1001388.
[10] L. Lonappan, S.L. Brar, R.K. Das, M. Verma, R.Y. Surampalli, Diclofenac and its transformation products: environmental occurrence and toxicity - a review, Environ. Int., 96 (2016) 127–138.
[11] S.E. Owumi, U.J. Dim, Biochemical alterations in diclofenac-treated rats: effect of selenium on oxidative stress, inflammation, and hematological changes, Toxicol. Res. Appl., (2019), doi: 10.1177/2397847319874359.
[12] M. Syed, C. Skonberg, S.H. Hansen, Mitochondrial toxicity of diclofenac and its metabolites via inhibition of oxidative phosphorylation (ATP synthesis) in rat liver mitochondria: possible role in drug induced liver injury (DILI), Toxicol. in Vitro, 31 (2016) 93–102.
[13] M. Schmidt, H.T. Sørensen, L. Pedersen, Diclofenac use and cardiovascular risks: series of nationwide cohort studies, BMJ, (2018) 362, doi: 10.1136/bmj.k3426.
[14] J. Lindsay Oaks, M. Gilbert, M.Z. Virani, R.T. Watson, C.U. Meteyer, B.A. Rideout, H.L. Shivaprasad, S. Ahmed, M.J.I. Chaudhry, M. Arshad, S. Mahmood, A. Ali, A.A. Khan, Diclofenac residues as the cause of vulture population decline in Pakistan, Nature, 42 (2004) 630–633.
[15] L. Fent, A.A. Weston, D. Caminada, Ecotoxicology of human pharmaceuticals, Aquat. Toxicol., 76 (2006) 122–159.
[16] D. Ogada, P. Shaw, R.L. Beyers, R. Buij, C. Murn, J.M. Thiollay, C.M. Beale, R.M. Holdo, D. Pomeroy, N. Baker, S.C. Krüger, A. Botha, M.Z. Virani, A. Monadjem, A.R.E. Sinclair, Another continental vulture crisis: Africa's vultures collapsing toward extinction, Conserv. Lett., 9 (2016) 89–97.
[17] European Commission – Directive 2013/39/EU of the European Parliament and of the Council of 12 August 2013 Amending Directives 2000/60/EC and 2008/105/EC as Regards Priority Substances in the Field of Water Policy. http://eur-lex.europa.eu/legalcontent/EN/TXT/PDF/?uri=CELEX:32013L0039&from=EN (Accessed October 2019).
[18] Y. Praveenkumarreddy, K. Vimalkumar, B.R. Ramaswamy, V. Kumar, R.K. Singhal, H. Basu, C.M. Gopal, K.E. Vandana, K. Bhat, H.N. Udayashankar, K. Balakrishna, Assessment of non-steroidal anti-inflammatory drugs from selected wastewater treatment plants of Southwestern India, Emerging Contam., 7 (2021) 43–51.
[19] M.J. McKie, S.A. Andrews, R.C. Andrews, Conventional drinking water treatment and direct biofiltration for the removal of pharmaceuticals and artificial sweeteners: a pilot-scale approach, Sci. Total Environ., 544 (2016) 10–17.
[20] E.S. Rigobello, A.D.B. Dantas, L. Di Bernardo, E.M. Vieira, Removal of diclofenac by conventional drinking water treatment processes and granular activated carbon filtration, Chemosphere, 92 (2013) 184–191.
[21] J. Rivera-Utrilla, M. Sánchez-Polo, M.Á. Ferro-García, G. Prados-Joya, R. Ocampo-Pérez, Pharmaceuticals as emerging contaminants and their removal from water. A review, Chemosphere, 93 (2013) 1268–1287.
[22] W.T. Vieira, M.B. de Farias, M.P. Spaolonzi, M.G.C. da Silva, M.G.A. Vieira, Endocrine-disrupting compounds: occurrence, detection methods, effects and promising treatment pathways—a critical review, J. Environ. Chem. Eng., 9 (2021) 104558, doi: 10.1016/j.jece.2020.104558.
[23] P. Westerhoff, Y. Yoon, S.A. Snyder, E.C. Wert, Fate of endocrine-disruptor, pharmaceutical, and personal care product chemicals during simulated drinking water treatment processes, Environ. Sci. Technol., 39 (2005) 6649–6663.
[24] Y. Yoon, P. Westerhoff, S.A. Snyder, E.C. Wert, Nanofiltration and ultrafiltration of endocrine disrupting compounds, pharmaceuticals and personal care products, J. Membr. Sci., 270 (2006) 88–100.
[25] D. Krajišnik, A. Daković, A. Malenović, M. Milojević-Rakić, V. Dondur, Ž. Radulović, J. Milić, Investigation of adsorption and release of diclofenac sodium by modified zeolites composites, Microporous Mesoporous Mater., 167 (2013) 94–101.
[26] J.L. Sotelo, G. Ovejero, A. Rodríguez, S. Álvarez, J. Galán, J. García, Competitive adsorption studies of caffeine and diclofenac aqueous solutions by activated carbon, Chem. Eng. J., 240 (2014) 443–453.
[27] V. Rakić, V. Rac, M. Krmar, O. Otman, A. Auroux, The adsorption of pharmaceutically active compounds from aqueous solutions onto activated carbons, J. Hazard. Mater., 282 (2015) 141–149.
[28] M.A. Rodrigo, O. Scaldione, C.A. Martinez-Huitle, Electrochemical Water and Wastewater Treatment, Butterworth-Heinemann, Holland, 2018.
[29] F. Cao, M. Zhang, S. Yuan, J. Feng, Q. Wang, W. Wang, Z. Hu, Transformation of acetaminophen during water chlorination treatment: kinetics and transformation products identification, Environ. Sci. Pollut. Res., 23 (2016) 12303–12311.
[30] M. Kråkström, S. Saeid, P. Tolvanen, N. Kumar, T. Salmi, L. Kronberg, P. Eklund, Identification and quantification of transformation products formed during the ozonation of the non-steroidal anti-inflammatory pharmaceuticals ibuprofen and diclofenac, Ozone: Sci. Eng., The J. Int. Ozone Assoc., 44 (2021) 157–171.
[31] M.H. Plumlee, B.D. Stanford, J.-F. Debroux, D. Cory Hopkins, S.A. Snyder, Costs of advanced treatment in water reclamation, Ozone: Sci. Eng., The J. Int. Ozone Assoc., 5 (2014) 485–495.
[32] S. de Boer, J. González-Rodríguez, J.J. Conde, M.T. Moreira, Benchmarking tertiary water treatments for the removal of micropollutants and pathogens based on operational and sustainability criteria, J. Water Process Eng., 46 (2022) 102587, doi: 10.1016/j.jwpe.2022.102587.
[33] V. Sundaram, K. Pagilla, T. Guarin, L. Li, R. Marfil-Vega, Z. Bukhari, Extended field investigations of ozone-biofiltration advanced water treatment for potable reuse, Water Res., 172 (2020) 115513, doi: 10.1016/j.watres.2020.115513.
[34] L.A. Al-Khateeb, S. Almotiry, M.A. Salam, Adsorption of pharmaceutical pollutants onto graphene nanoplatelets, Chem. Eng. J., 248 (2014) 191–199.
[35] N. Suriyanon, P. Punyapalakul, C. Ngamcharussrivichai, Mechanistic study of diclofenac and carbamazepine adsorption on functionalized silica-based porous materials, Chem. Eng. J., 214 (2013) 208–218.
[36] S.-W. Nam, C. Jung, H. Li, M. Yu, J.R.V. Flora, L.K. Boateng, N. Her, K.-D. Zoh, Y. Yoon, Adsorption characteristics of diclofenac and sulfamethoxazole to graphene oxide in aqueous solution, Chemosphere, 136 (2015) 20–26.
[37] F.A. Rosli, H. Ahmad, K. Jumbri, A.H. Abdullah, S. Kamaruzaman, N.A.F. Abdullah, Efficient removal of pharmaceuticals from water using graphene nanoplatelets as adsorbent, R. Soc. Open Sci., (2021), doi: 10.1098/rsos.201076.
[38] W.S. Hummers Jr., R.E. Offeman, Preparation of graphitic oxide, J. Am. Chem. Soc., 80 (1958) 1339, doi: 10.1021/ja01539a017.
[39] S. Lagergren, About the theory of so-called adsorption of soluble substances, Kungliga Svenska Vetenskapsakademiens, Handlingar, 24 (1898) 1–39.
[40] Y.S. Ho, G. McKay, Pseudo-second order model for sorption processes, Process Biochem., 34 (1999) 451–465.
[41] W.K. Webber, J.C. Morris, Kinetics of adsorption on carbon from solutions, J. Sanit. Eng. Div., Am. Soc. Civ. Eng., 89 (1963) 31–60.
[42] I. Langmuir, The adsorption of gases on plane surfaces of glass, mica and platinum, J. Am. Chem. Soc., 40 (1918) 1361–1403.
[43] H.M.F. Freundlich, Over the adsorption in solution, J. Phys. Chem., 57 (1906) 385–471.
[44] R.K. Singh, R. Kumar, D.P. Singh, Graphene oxide: strategies for synthesis, reduction and frontier applications, RSC Adv., 6 (2016) 64993–65011.

[45] B.Y.Z. Hiew, L.Y. Lee, X.J. Lee, S. Gan, S. Thangalazhy-Gopakumar, S.S. Lim, G.-T. Pan, T.C.-K. Yang, Adsorptive removal of diclofenac by graphene oxide: optimization, equilibrium, kinetic and thermodynamic studies, J. Taiwan Inst. Chem. Eng., 98 (2019) 150–163.
[46] C. Bartlam, S. Morsch, K.W.J. Heard, P. Quayle, S.G. Yeates, A. Vijayaraghavan, Nanoscale infrared identification and mapping of chemical functional groups on graphene, Carbon, 139 (2018) 317–324.
[47] S.-G. Kim, O.-K. Park, J.H. Lee, B.-C. Ku, Layer-by-layer assembled graphene oxide films and barrier properties of thermally reduced graphene oxide membranes, Carbon Lett., 14 (2013) 247–250.
[48] M.P. More, P.K. Deshmukh, Quality by design approach for the synthesis of graphene oxide nanosheets using full factorial design with enhanced delivery of Gefitinib nanocrystals, Mater. Res. Express, 8 (2021) 075602, doi: 10.1088/2053-1591/ac144b.
[49] R. Hack, C.H.G. Correia, R.A.D.S. Zanon, S.H. Pezzin, Characterization of graphene nanosheets obtained by a modified Hummer's method, Matéria (Rio de Janeiro), 23 (2018), doi: 10.1590/S1517-707620170001.0324.
[50] Y.J. Yun, W.G. Hong, W.-J. Kim, Y. Jun, B.H. Kim, A novel method for applying reduced graphene oxide directly to electronic textiles from yarns to fabrics, Adv. Mater., 25 (2013) 5701–5705.
[51] K. Khanafer, K. Vafai, Analysis of the anomalies in graphene thermal properties, Int. J. Heat Mass Transfer, 104 (2017) 328–336.
[52] J.-F. Dai, G.-J. Wang, L. Ma, C.-K. Wu, Surface properties of graphene: relationship to graphene-polymer composites, Rev. Adv. Mater. Sci., 40 (2015) 60–71.
[53] W. Luo, C. Bommier, Z. Jian, X. Li, R. Carter, S. Vail, Y. Lu, J.-J. Lee, X. Ji, Low-surface-area hard carbon anode for Na-ion batteries via graphene oxide as a dehydration agent, ACS Appl. Mater. Interfaces, 4 (2015) 2626–2631.
[54] A. Ariharan, B. Viswanathan, V. Nandhakumar, Nitrogen doped graphene as potential material for hydrogen storage, Graphene, 6 (2017) 41–60.
[55] A. Sheikhmohammadi, S.M. Mohseni, R. Khodadadi, M. Sardar, M. Abtahi, S. Mahdavi, H. Keramati, Z. Dahaghin, S. Rezaei, M. Almasian, M. Sarkhosh, M. Faraji, S. Nazari, Application of graphene oxide modified with 8-hydroxyquinoline for the adsorption of Cr(VI) from wastewater: optimization, kinetic, thermodynamic and equilibrium studies, J. Mol. Liq., 233 (2017) 75–88.
[56] G. Torgut, M. Tanyol, F. Biryan, G. Pihtili, K. Demirelli, Application of response surface methodology for optimization of Remazol Brilliant Blue R removal onto a novel polymeric adsorbent, J. Taiwan Inst. Chem. Eng., 80 (2017) 406–414.
[57] A. Afkhami, M. Saber-Tehrani, H. Bagheri, Modified maghemite nanoparticles as an efficient adsorbent for removing some cationic dyes from aqueous solution, Desalination, 263 (2017) 240–248.
[58] R. Rostamian, H.A. Behnejad, A comprehensive adsorption study and modeling of antibiotics as a pharmaceutical waste by graphene oxide nanosheets, Ecotoxicol. Environ. Saf., 147 (2018) 117–123.
[59] Drugbank – Diclofenac. Available at: https://go.drugbank.com/drugs/DB00586 (Accessed April 2020).
[60] C. Saucier, M.A. Adebayo, E.C. Lima, R. Catalunã, P.S. Thue, L.D.T. Prola, M.J. Puchana-Rosero, F.M. Machado, F.A. Pavan, G.L. Dotto, Microwave-assisted activated carbon from cocoa shell as adsorbent for removal of sodium diclofenac and nimesulide from aqueous effluents, J. Hazard. Mater., 289 (2015) 18–27.
[61] A. Molla, Y. Li, B. Mandal, S.G. Kang, S.H. Hur, J.S. Chung, Selective adsorption of organic dyes on graphene oxide: theoretical and experimental analysis, Appl. Surf. Sci., 464 (2019) 170–177.
[62] S. Azizian, Kinetic models of sorption: a theoretical analysis, J. Colloid Interface Sci., 276 (2004) 47–52.
[63] W. Plazinski, J. Dziuba, W. Rudzinski, Modeling of sorption kinetics: the pseudo-second order equation and the sorbate intraparticle diffusivity, Adsorption, 19 (2013) 1055–1064.
[64] V.C. Silva, M.E.B. Araújo, A.M. Rodrigues, J.M. Cartaxo, R.R. Menezes, G.A. Neves, Adsorption behavior of acid-treated Brazilian palygorskite for cationic and anionic dyes removal from the water, Sustainability, 13 (2021) 3954, doi: 10.3390/su13073954.
[65] C.H. Giles, T.H. MacEwan, S.N. Nakhwa, D. Smith, Studies in adsorption. Part XI. A system of classification of solution adsorption isotherms, and its use in diagnosis of adsorption mechanisms and in measurement of specific surface areas of solids, J. Chem. Soc., (1960) 3973–3993, doi: 10.1039/JR9600003973.
[66] M. Thommes, K. Kaneko, A.V. Neimark, J.P. Olivier, F. Rodriguez-Reinoso, J. Rouquerol, K.S.W. Sing, Physisorption of gases, with special reference to the evaluation of surface area and pore size distribution (IUPAC Technical Report), Pure Appl. Chem., 87 (2015), doi: 10.1515/pac-2014-1117.
[67] M.D.G. de Luna, Murniati, W. Budianta, K.K.P. Rivera, R.O. Arazo, Removal of sodium diclofenac from aqueous solution by adsorbents derived from cocoa pod husks, J. Environ. Chem. Eng., 5 (2017) 1465–1474.
[68] I.M. Jauris, C.F. Matos, C. Saucier, E.C. Lima, A.J.G. Zarbin, S.B. Fagan, F.M. Machado, I. Zanella, Adsorption of sodium diclofenac on graphene: a combined experimental and theoretical study, Phys. Chem. Chem. Phys., 8 (2016) 1526–1536.
[69] N. Thi Minh Tam, Y. Liu, H. Bashir, Z. Yin, Y. He, X. Zhou, Efficient removal of diclofenac from aqueous solution by potassium ferrate-activated porous graphitic biochar: ambient condition influences and adsorption mechanism, Int. J. Environ. Res. Public Health, 17 (2019) 291, doi: 10.3390/ijerph17010291.
[70] T. Liu, Z. Xie, Y. Zhang, J. Fan, Q. Liu, Preparation of cationic polymeric nanoparticles as an effective adsorbent for removing diclofenac sodium from water, RSC Adv., 7 (2017) 38279–38286.
[71] F. Jiang, D. Zhang, X.-k. Ouyang, L.-Y. Yang, Fabrication of porous polyethyleneimine-functionalized chitosan/Span 80 microspheres for adsorption of diclofenac sodium from aqueous solutions, Sustainable Chem. Pharm., 21 (2021) 100418, doi: 10.1016/j.scp.2021.100418.
[72] I. Duru, D. Ege, A.R. Kamali, Graphene oxides for removal of heavy and precious metals from wastewater, J. Mater. Sci., 51 (2016) 6097–6116.